Functional expression of the ATP-gated P2X7 receptor in human iPSC-derived neurons and astrocytes

Jaideep Kesavan[1], Orla Watters[1,4], Klaus Dinkel[2], Michael Hamacher[3], Jochen H.M. Prehn[1,4], David C. Henshall[1,4] and Tobias Engel[1,4]*

[1]Department of Physiology & Medical Physics, Royal College of Surgeons in Ireland, University of Medicine and Health, Dublin D02 YN77, Ireland

[2]Lead Discovery Center GmbH, Otto-Hahn-Straße 15, 44227 Dortmund, Germany

[3]Affectis Pharmaceuticals AG, Otto-Hahn-Straße 15, 44227 Dortmund, Germany

[4]FutureNeuro, Science Foundation Ireland Research Centre for Chronic and Rare Neurological Diseases, RCSI, Dublin D02 YN77, Ireland

*Correspondence: Tobias Engel, Ph.D., Department of Physiology & Medical Physics, Royal College of Surgeons in Ireland, 123 St. Stephen's Green, Dublin 2, Ireland.

Tel: +35314025199 Fax: +35314022447, Email: _tengel@rcsi.ie_

Abstract

The P2X7 receptor (P2X7R) is a cation membrane channel activated by extracellular adenosine 5'-triphosphate. Activation of this receptor results in numerous downstream events including the modulation of neurotransmission, release of pro-inflammatory mediators, cell proliferation or cell death. While the expression of P2X7Rs is well documented on microglia and oligodendrocytes, the presence of functional P2X7Rs on neurons and astrocytes remains debated. Furthermore, to date, functional studies on the P2X7R are mostly limited to studies in cells from rodents and immortalised cell lines expressing human P2X7Rs. To assess the functional expression of P2X7Rs in human neurons and astrocytes, we differentiated human-induced pluripotent stem cells (hiPSCs) into forebrain cortical neurons that co-express FOXG1 and βIII-tubulin as well as S100 β-expressing astrocytes. Immunostaining revealed prominent punctate P2X7R staining on the soma and processes of hiPSC-derived neurons and astrocytes. In addition, our data show that stimulation with the potent nonselective P2X7R agonist BzATP induces robust calcium rises in hiPSC-derived neurons and astrocytes, which were blocked by the selective P2X7R antagonist AFC-5128. Together, our findings provide evidence for the functional expression of P2X7Rs in hiPSC-derived forebrain cortical neurons and astrocytes demonstrating that these cells offer the potential for investigating P2X7R-mediated pathophysiology and drug screening *in vitro*.

Keywords: P2X7 receptor, human iPSC-derived neurons and glia, BzATP-evoked Ca^{2+} fluctuations

1. Introduction

The ATP-gated purinergic P2X7 receptor (P2X7R) plays a pivotal role in ATP-mediated signal transmission in the brain. ATP may be released from nerve terminals or glial cells by exocytosis [1] or from astroglial cells via non-exocytotic mechanisms. ATP has also been shown to leak through the damaged neuronal or glial plasma membrane during brain injury [2, 3]. When ATP binds to the extracellular domain of the P2X7R, the channel opens allowing the permeation of small cations such as Na^+, Ca^{2+}, and K^+ [4]. In addition, P2X7Rs are also believed to form a non-selective "macro pore" which allows the influx of large-molecular-weight molecules [4]. Activation of P2X7R evokes glutamate release from presynaptic nerve terminals and from astrocytes leading to excitotoxic effects [5], while activation of P2X7R on astrocytes and microglia has been shown to lead to the release of Interleukin-1β (IL-1β), IL-6, and Tumor necrosis factor-α (TNF-α), triggering neuroinflammation [6]. The P2X7R has attracted considerable interest as a potential target for various central nervous system (CNS) disorders including epilepsy, and neurodegenerative diseases such as Parkinson's disease, Alzheimer's disease and multiple sclerosis as well as non-CNS diseases such as migraine and neuropathic pain [7-9]. P2X7R protein expression has been found to be highly up-regulated in the brain of patients with neurological diseases such as Huntington's disease [10], intractable temporal lobe epilepsy (TLE) [11] and in cortical lesions of patients with focal cortical dysplasia [12].

Despite the 80% sequence homology between human and murine P2X7Rs, differences in the receptor sensitivity towards various ligands have been described. For example, the human P2X7R has been shown to be 10–100 times more sensitive to the non-selective agonist 2',3'-O-(benzoyl-4-benzoyl)-adenosine 5'- triphosphate (BzATP) compared to the murine ortholog [13-15]. KN-62 (1-[N,O-bis(5-isoquinolinesulphonyl)-N-methyl-L-tyrosyl]-4-phenylpiperazine), a potent antagonist for human P2X7Rs has been shown to be inefficacious at rat P2X7Rs [16]. Likewise, human P2X7Rs subjected to ivermectin underwent positive allosteric modulation while modest results were seen at rodent P2XRs, suggesting a species-specific mode of action [17]. Thus, P2X7Rs exhibit remarkable species-specific differences in the pharmacological properties including agonist and antagonist potency and sensitisation which could account for the failure in clinical translation of the results from animal models [13]. Consequently, there is an increasing need for the investigation of the expression

83 and function of P2X7Rs in human brain-relevant models. Resected human primary brain tissue is
84 very scarce and often shows alterations associated with pathology. Advances in human induced
85 pluripotent stem cell (hiPSC) technology has led to the differentiation of region-specific human
86 neurons, astrocytes, oligodendrocytes and microglia from somatic cells [18-21]. These iPSC-derived
87 human neurons and glia have demonstrated tremendous potential for the investigation of human
88 neuronal development *in vitro*, pharmacological screening and assessing phenotypic alterations in
89 patient-specific iPSC-derived neural cells [22-27].
90
91 To date, only a few studies have addressed the functional expression of the P2X7R in human
92 neurons and astrocytes compared with work on rodent counterparts [28-30]. The main purpose of
93 this study was to characterize the functional expression of P2X7Rs in hiPSC-derived neurons and
94 astrocytes. Here, we demonstrate the expression of P2X7Rs using immunocytochemical analysis and
95 BzATP-evoked Ca^{2+} transients in hiPSC-derived neurons and astrocytes.
96

97 **2. Materials and Methods**

98 **Culture and Differentiation of hiPSCs**
99 hiPSCs HPSI0114i-eipl_1 (ECACC 77650081; Culture Collections, Public Health England, UK) at
100 passage 32 were maintained under feeder-free conditions on vitronectin (STEMCELL Technologies,
101 British Columbia, Canada)-coated 6-well plates in E8 medium (Thermo Fisher Scientific, Massachusetts,
102 USA). hiPSCs were dissociated by using 0.5 mM EDTA for 2 min at 37°C, and reseeded at the density
103 of 1×10^4 cells per cm². Cortical differentiation of hiPSCs was carried out as described previously, with
104 minor modifications [31]. For the neural induction of hiPSCs, approximately 24 h after splitting, culture
105 medium was switched to Gibco PSC Neural Induction Medium (Thermo Fisher Scientific,
106 Massachusetts, U.S.A.) containing Neurobasal medium and Gibco PSC neural induction supplement.
107 Neural induction medium was changed every other day from day 0 to day 4 of neural induction and
108 every day thereafter. At day 10 of neural induction, primitive NSCs (pNSCs) were dissociated with
109 Accutase (Thermo Fisher Scientific, Massachusetts, USA) and plated on Geltrex-coated dishes at a
110 density of 1×10^5 cells per cm² in NSC expansion medium containing 50% Neurobasal medium, 50%
111 Advanced DMEM/F12, and 1% neural induction supplement (Thermo Fisher Scientific, Massachusetts,
112 U.S.A.). pNSCs were passaged on the 4th day at a 1:3 split ratio to derive NSCs and cells at passage 4
113 were used for the differentiation of neurons and glia. For the differentiation of neurons, NSCs were
114 plated on Geltrex-coated coverslips at a density of 5×10^4 cells per cm² in neuronal differentiation
115 medium consisting of neurobasal medium and DMEM-F12 (1:1), with 2% B-27 supplement, 1% N2
116 supplement, 1% L-glutamine, 1% nonessential animal acids, 20 ng/ml brain-derived neurotrophic factor
117 (BDNF), 20 ng/ml glial cell-derived neurotrophic factor (GDNF) (all from Thermo Fisher Scientific,
118 Massachusetts, USA), 100 ng/mL cAMP, 100 μM L-ascorbic acid and penicillin/streptomycin (all from
119 Merck, Missouri, United States). The culture medium was changed every 2–3 days. For astrocyte
120 differentiation, pNSCs were plated onto Geltrex-coated coverslips at a density of 5×10^4 cells per cm² in
121 an astrocyte differentiation medium (DMEM supplemented with 1% fetal bovine serum, 1% sodium
122 pyruvate, 1% non-essential amino acids, 0.5% G-5 supplement (all from Thermo Fisher Scientific,
123 Massachusetts, USA)) for 5 days. The astrocytes were passaged at a split ratio of 1:2 and medium was
124 changed every 3 days. Astrocytes at passage 7 to 9 were used for experiments.
125

126 **Immunocytochemistry**
127 NSCs, neurons and astrocytes cultured on coverslips were fixed with 4% paraformaldehyde for
128 15 min. After 3 washes in phosphate buffered saline, cells were permeabilized with 0.1% Triton for
129 20 min and blocked in 1% BSA for 30 min. Cells were incubated at 4°C overnight in primary antibody
130 diluted in 1% BSA. The cells were then incubated in secondary antibody diluted in 1% BSA for 1 h at
131 room temperature. The following primary antibodies were used: mouse anti-SOX2 (R&D Systems,
132 Minneapolis, MN, USA), rabbit anti-nestin, mouse anti-PAX6, rabbit anti-FOXG1 (all from Abcam,

3

133   Cambridge, UK), mouse anti-β-tubulin III (Biolegend, San Diego, CA) and rabbit anti-P2X7R (Alomone
134   Labs, Jerusalem, Israel). The respective secondary antibodies were conjugated to Alexa Fluor 488 or
135   Alexa Fluor 594 (Thermo Fisher Scientific, Massachusetts, USA). Coverslips were mounted and images
136   were acquired using a Leica DM4 B fluorescence microscope.
137

138 **Patch-clamp electrophysiology**
139   NSC-derived neurons differentiated for 2–8 weeks *in vitro* were selected for patch-clamp
140   experiments. Whole cell voltage-clamp recording was carried out with a Multiclamp 700 B amplifier
141   (Molecular Devices, California, USA) which was interfaced by an A/D-converter (Digidata 1550B,
142   Molecular Devices, California, USA) to a PC running pClamp software (Version 11, Molecular Devices,
143   California, USA). The signals were low-pass filtered at 2 kHz or 10 kHz and sampled at 10 kHz or 50
144   kHz. Pipette electrodes (G150T-4, Hardward Apparatus, Massachusetts, USA) were fabricated using a
145   vertical puller (Narishige PC-100, Tokyo, Japan). All recordings were performed at 32°C in a bath
146   solution containing (in mM): 135 NaCl, 3 KCl, 2 CaCl2, 1 MgCl2, 10 Hepes and 10 glucose (pH 7.2;
147   osmolality 290–300 mmol/kg). For recordings of currents, the patch pipette contained the following
148   solution (in mM): 120 potassium gluconate, 20 KCl, 10 NaCl, 10 EGTA, 1 CaCl2, 4 Mg ATP, and 0.4 Na
149   GTP, and 10 HEPES (pH 7.2, osmolality 280–290 mmol/kg). Spontaneous action potential firing was
150   detected in loose-patch configuration with patch pipettes filled with the bath solution.
151

152 **Drug application**
153   Stock solutions of BzATP (Alomone Labs, Jerusalem, Israel) and AFC-5128 (Affectis
154   Pharmaceuticals AG, Dortmund, Germany) were diluted and applied in HEPES-buffered extracellular
155   solution. The drug solutions were delivered to the recorded cells by a valve-controlled fast multibarrel
156   superfusion system with a common outlet approximately 350 μm in diameter (Automate Scientific,
157   California, USA). The application tip was routinely positioned approximately 1 mm away from and
158   ~50 μm above the surface of the recorded cells. A computer connected to Digidata 1550B controlled the
159   onset and duration of each drug application. The time course of the drug application was calibrated
160   using fluorescein dye.
161

162 **Calcium Imaging**
163   Cells were loaded at 37°C with fluo-4 (Abcam, Cambridge, UK) or Cal-520 (AAT Bioquest,
164   California, USA) by incubation with the acetoxymethyl (AM) ester form of the dye at a final
165   concentration of 2 μM in culture media. After 45 min, cells were washed several times with dye-free
166   HEPES-buffered saline solution and transferred to an imaging chamber on a microscope (Zeiss Axio
167   Examiner, Jena, Germany) equipped with a Zeiss 40x water immersion objective. Zen Blue imaging
168   software (Carl Zeiss, Jena, Germany) was used for hardware control and image acquisition, and image
169   analysis was performed using ImageJ (NIH, Maryland, USA). All imaging experiments were performed
170   at 32°C in a low divalent cation containing bath solution with the composition (in mM): 135 NaCl, 3
171   KCl, 0.1 CaCl2, 0 MgCl2, 10 HEPES and 10 glucose (pH 7.2; osmolality 290–300 mmol/kg). Images were
172   acquired at 4 Hz. Background fluorescence was measured from the cell-free area outside the soma of
173   interest in each frame of every time series. Region of interests (ROIs) were manually drawn around the
174   soma and baseline fluorescence intensity (F0) was determined by averaging 14 frames preceding the
175   cell's exposure to BzATP, and the time course of normalized fractional dye fluorescence [ΔF/F0] was
176   obtained, where ΔF equals F(t)- F0.
177

178 **Data analysis**
179   The data are expressed as mean ± SEM. Statistical analysis was performed by Student's t- test.
180     $P < 0.05$ was considered statistically significant. All statistical analysis was performed with GraphPad
181   Prism 9 software (GraphPad Software, San Diego, CA, USA).
182
183

4

3. Results

3.1. Differentiation of forebrain cortical neurons and astrocytes from hiPSC-derived primitive neural stem cells.

In order to assess the functional expression of P2X7Rs in a human brain-relevant cellular model, we differentiated cortical neurons and astrocytes from hiPSCs that were maintained on vitronectin-coated plates in E8 medium for 2 passages. The hiPSCs were passaged with 0.5 mM EDTA at a split ratio of 1:5. Cells maintained under these conditions were characterized by undifferentiated morphology with round and clear edges (Figure 1A).
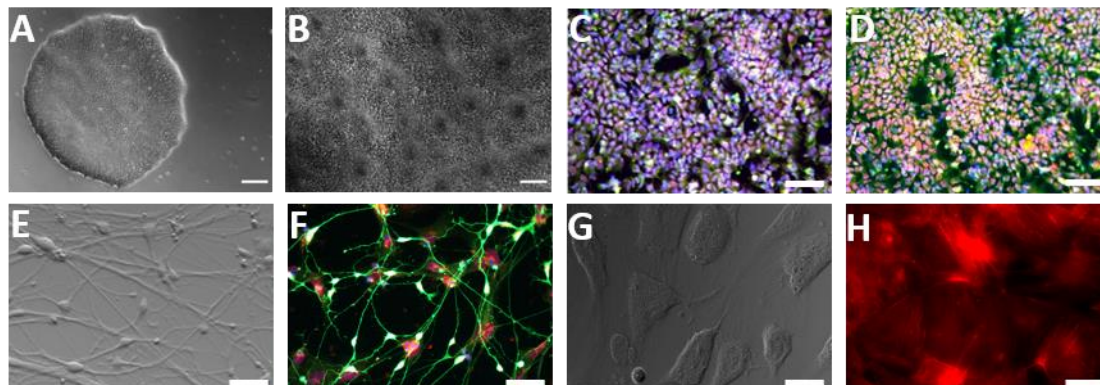

Figure 1. Differentiation of forebrain neurons from hiPSCs. (**A**) Brightfield image of hiPSC colony cultured in feeder-free conditions at day 3 *in vitro*. (**B**) pNSCs derived from hiPSCs at day 7. (**C**) Expression of neural stem/progenitor markers nestin (green) and SOX2 (red) in NSCs. Cell nuclei were stained with Hoechst (blue). (**D**) The NSCs co-express neural stem/progenitor markers nestin (green) and dorsal telencephalic progenitor marker PAX6 (red). Cell nuclei were stained with Hoechst (blue). (**E**) NSC-derived neurons at two weeks of differentiation *in vitro*. (**F**) Differentiated cells were stained with antibodies against the forebrain marker FOXG1 (red) and the neuronal marker, β-III tubulin (green). Cell nuclei were stained with Hoechst (blue). (**G**) Brightfield image of differentiated pNSCs in astrocyte induction media. (**H**) Differentiated astrocytes express astrocyte marker S100β. Scale bars 100 μm (A, B, C and D) or 50 μm (E, F, G and H).

Next, we differentiated hiPSCs to primitive neural stem cells by dissociating the hiPSC colonies using accutase and plating onto Geltrex-coated dishes in neural induction medium for 10 days resulting in a population of pre-NSCs (Figure 1B). The medium was changed every other day for the first 4 days and every day thereafter. Once confluent, cells were passaged 1:3 and could be cryopreserved in liquid nitrogen. At passage 4, the cells exhibited a homogeneous morphology and immunocytochemical analysis revealed the expression of specific markers of mature NSCs such as Nestin, SOX2 (Figure 1C) and the dorsal telencephalic progenitor marker PAX6 (Figure 1D). For neuronal differentiation, NSCs at passage 4 were plated on Geltrex-coated plates in neuronal differentiation medium. At 14 days *in vitro*, cells exhibited neuronal morphology and were positive for the neuron-specific cytoskeletal marker β-III-tubulin and forebrain marker FOXG1 (Figure 1E-F). For the differentiation of astrocytes, dissociated NSCs were plated onto Geltrex-coated plates at a density of 5×10^4 cells per cm^2 in an astrocyte differentiation medium and confluent cultures were passaged every 4-5 days at a ratio of 1:2, and medium was changed every 2–3 days. Immunocytochemical analysis at passage 7 confirmed the expression of the astrocyte marker S100β in cells maintained in astrocyte differentiation mediaum (Figure 1 G-H).

Thus, our data demonstrate efficient induction of pNSCs with the potential for differentiation into forebrain cortical neurons and astrocytes.

3.2. In vitro differentiated hiPSC-derived cortical neurons exhibit fundamental electrophysiological properties.

5

219   For the functional assessment of the differentiated neurons, NSCs were plated on a monolayer
220   of hiPSC-derived astrocytes from the same hiPSC line and maintained for 2 to 8 weeks. Using whole-
221   cell patch-clamp recordings from individual neurons, we first confirmed that NSC-derived cortical
222   neurons differentiate as functional neurons exhibiting fundamental electrophysiological properties.
223   The recordings demonstrated the presence of fast activating and inactivating inward currents and
224   slow and sustained outward currents resembling voltage-gated Na^+ (Na_v) and K^+ (K_v) channels
225   (Figure 2 A-B).
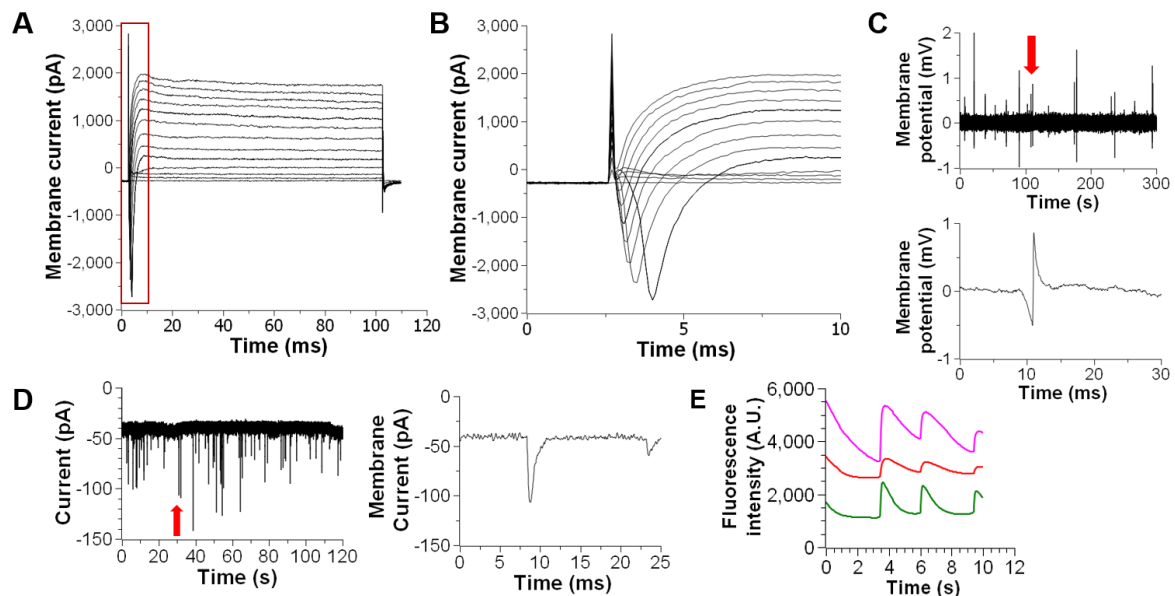

227   **Figure 2**. Fundamental electrophysiological properties of hiPSC-derived neurons. (**A**) Representative traces of
228   fast-inactivating inward currents and sustained outward currents recorded in voltage-clamp mode. (**B**)
229   Expanded view of the boxed region of inward and outward currents. (**C**) Action potentials recorded in loose-
230   patch configuration. One action potential indicated by the red arrow is shown at expanded scale at the bottom.
231   (**D**) Spontaneous postsynaptic currents (sPSCs) recorded in whole-cell configuration from hiPSC-derived neural
232   network. Expanded view of the sPSC (right). (**E**) Example of spontaneous synchronized $[Ca^{2+}]_i$ transients in Fluo-
233   4 loaded neurons.

234   Demonstrating neuronal maturity, non-permeating loose-patch recordings confirmed
235   spontaneous action potential firing of neurons (Figure 2C). Another hallmark of a mature neuronal
236   network is the formation of functional synapses. Whole-cell voltage clamp recordings revealed
237   spontaneous postsynaptic currents (sPSCs) at 21-28 days *in vitro* differentiation (Figure 2D). In
238   addition, synchronous Ca^{2+} transients measured by oscillations in Fluo-4 fluorescence were also
239   evident in differentiated neurons indicating a synaptically connected network (Figure 2E).
240   Therefore, pNSCs terminally differentiate to neurons *in vitro* and exhibit fundamental
241   electrophysiological properties including action potential firing and synaptic transmission.
242
243   *3.3. Expression of P2X7Rs in hiPSC-derived neurons and astrocytes*
244   To investigate if P2X7Rs are expressed in hiPSC-derived neurons, immunocytochemistry was
245   performed at 8 h after plating the NSCs. At this stage, the differentiated cells with neuronal
246   morphology expressed the neuronal marker β-III tubulin (Figure 3 A,B). In double-labelling
247   experiments using the neuronal marker β-III tubulin and P2X7R-specific affinity purified antibody,
248   expression of P2X7Rs was evident by a punctate staining pattern (Figure 3 C-D). Notably, the β-III
249   tubulin antibody produced a more diffuse cellular staining compared to the noticeable punctate
250   staining in the neuronal soma and along the processes by the P2X7R-specific antibody. Likewise, to
251   assess the expression of P2X7Rs on hiPSC-derived astrocytes, double immunostaining was
6

252 performed on astrocytes at 4 weeks *in vitro* using antibodies against the astrocyte marker GFAP and
253 P2X7R. The punctate staining pattern for P2X7R was also present in GFAP-positive cells
254 demonstrating the expression of P2X7Rs in astrocytes (Figure 3 E-H).
255
256 These results demonstrate the expression of P2X7Rs on hiPSC-derived neuronal soma and
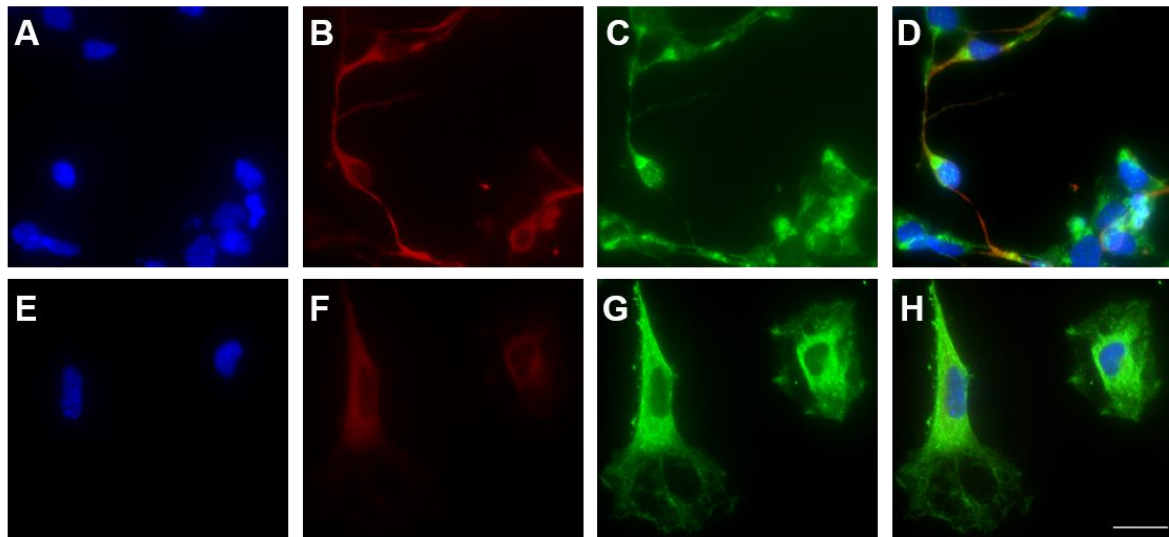257 processes as well as on astrocytes.
258

260 **Figure 3.** Immunofluorescence analysis of P2X7R expression in hiPSC-derived neurons and astrocyes. (**A–D**)
261 Immunofluorescence analysis of neurons stained with an antibody against P2X7R (green) with double-labelling
262 using neuronal marker β-III tubulin (red). (**E–H**) Immunofluorescence analysis of astrocyte marker GFAP. The
263 nucleus is counterstained with Hoechst (blue). Note the punctate co-localization of P2X7R immunoreactivity
264 with β -III tubulin or GFAP. Scale bar 50 μM.
265

266 *3.3. BzATP evokes AFC-5128-sensitive Ca^{2+} transients in hiPSC-derived neurons*

267 To confirm the results obtained using immunocytochemistry, we next sought to assess whether
268 P2X7Rs also respond to the application of P2X7R-stimulating agonists. Normally, the activation of
269 the P2X7R requires high (in mM range) concentrations of ATP. The P2X7R is, however, 10 to 30 times
270 more sensitive to the ATP analog and unselective P2X7R agonist, 2',3'-O-(4-benzoylbenzoyl)-ATP
271 (BzATP) [32, 33]. To assess the functional expression of P2X7Rs, hiPSC-derived neurons grown on
272 coverslips were loaded with 2 μM Cal-520 AM calcium-sensitive fluorescent dye. Unstimulated
273 neurons bathed in extracellular Cal-520 solution showed a measurable level of Cal-520 fluorescence
274 (excitation 494 nm: emission 525 nm), indicating resting [Ca^{2+}]i (Figure 3A).
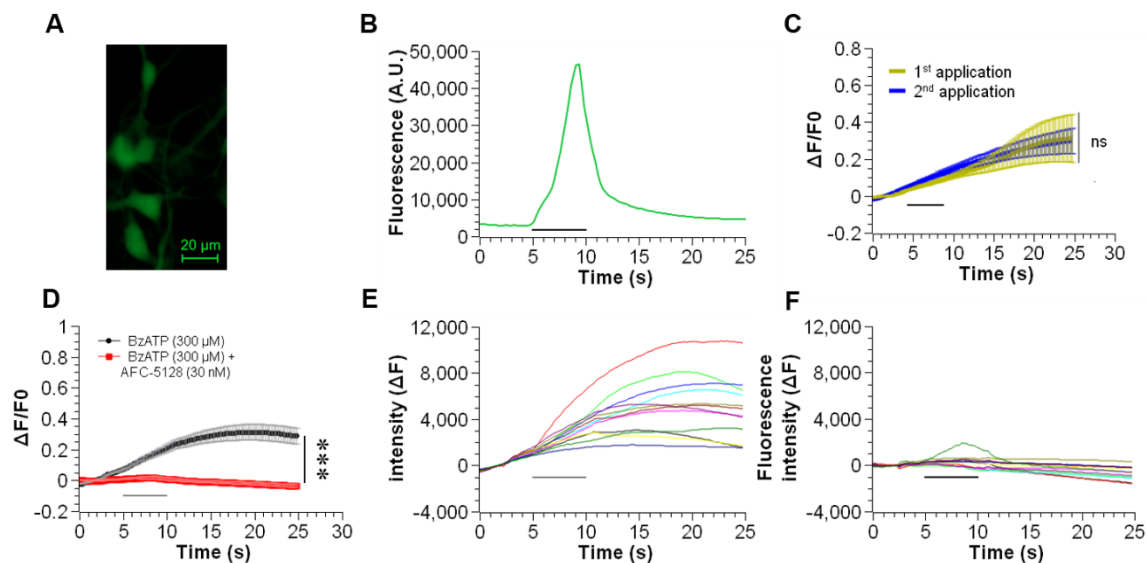
7

Figure 4. BzATP-evoked Ca^{2+} responses in hiPSC-derived neurons. (A) Representative image of Cal-520-loaded hiPSC-derived neurons at rest. (B) Graph illustrating the time course of fluorescein dye calibration. (C) BzATP-evoked calcium responses to two consecutive applications of 300 µM BzATP (Paired t-test, p> 0.05 (n = 8). (D) Response to the application of BzATP (300 µM) in the abcence (black trace) and presence (red trace) of the P2X7R antagonist AFC-5128 (30 nM). The values represent the mean and SEM. (Paired t-test, ***p < 0.001 (n = 14). (E) Traces illustrating BzATP -evoked calcium fluorescence response of individual neurons in the abcence of AFC-5128. (F) Traces illustrating BzATP -evoked calcium fluorescence response of individual neurons in the presence of AFC-5128.

The duration and time-course of the drug application was calibrated using fluorescein dye that was programmed to start at 5 s after the ejection of the control solution and continue to flow for a duration of 5 s. Analysis of the time-course of the fluorescein dye application confimed that the dye followed the preset stipulated time-couse (Figure 3B). During two consecutive appications of 300 µM BzATP, hiPSc-derived neurons responded to each application by a discernable increase in fluorescence (Figure 3C). To assess if the BzATP-evoked responses are P2X7R mediated, we repeated the BzATP application in the presence of the P2X7R antagonist AFC-5128 [34]. Fluorescence rose quickly in response to a pulse of 300 µM BzATP for 5 s signifying a persistent rise in [Ca^{2+}]i during constant agonist exposure. In contrast, when the cells were pre-incubated with the P2X7R antagonist AFC-5128 (30 nM) pulse ejection of 300 µM BzATP and 30 nM AFC-5128 the change in [Ca^{2+}]i was significantly reduced (Figure 3D). Individual neurons exhibited a synchronous increase in Cal-520 fluresence (ΔF) upon application of the agonist BzATP (Figure 3E) which was markedly reduced in the presence of the P2X7R inhibitior AFC-5128 (Figure 3F).

Taken together, these results show that the BzATP-gated change in [Ca^{2+}]i in hiPSC-derived neurons is mediated via the P2X7R.

3.4. BzATP evokes AFC-5128-sensitive Ca^{2+} transients in iPSC-derived astrocytes

Similar to neurons, we then assessed the functional expression of P2X7Rs in hiPSC-derived astrocytes by monitoring changes in [Ca^{2+}]i upon BzATP application, using the calcium-sensitive fluorescent reporter Cal-520. Unstimulated astrocytes bathed in extracellular solution showed a dim but measurable level of Cal-520 fluorescence (excitation 494 nm: emission 525 nm), indicating low resting [Ca^{2+}]i (Figure 4A). The hiPSC-derived astrocytes exhibited spontaneous asynchronous [Ca^{2+}]i fluctuations (Figure 4B). Similar to our findings in hiPSC-derived neurons, pulse ejection of BzATP (300 µM) for 5 s evoked an increase in [Ca^{2+}]i in a population of hiPSC-derived astrocytes (Figure 4C).
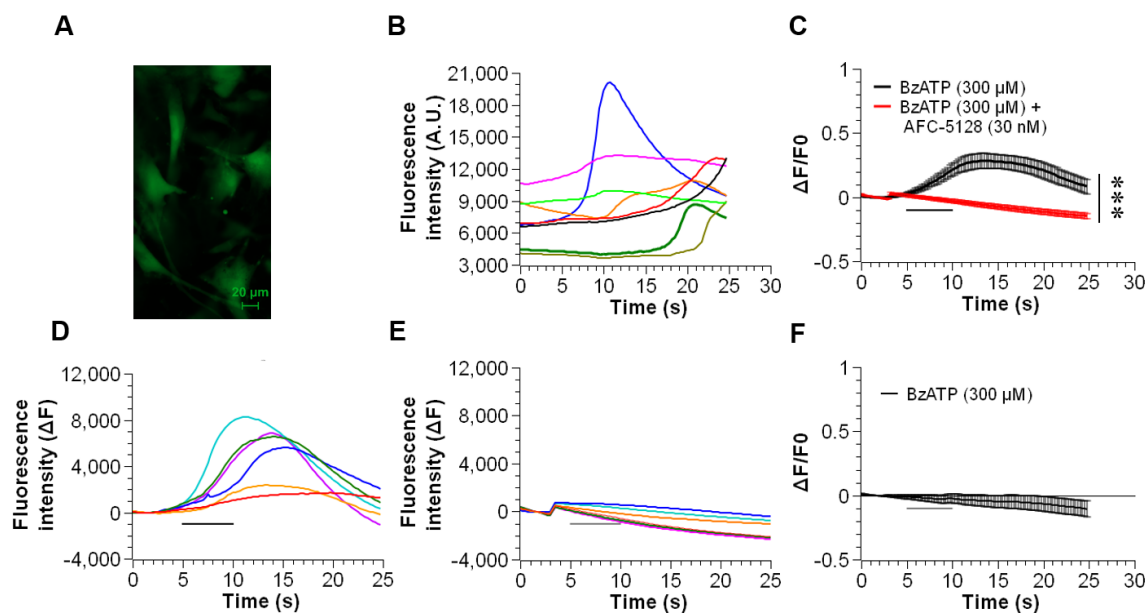
8

308

309

Figure 5. BzATP-evoked Ca2+ responses in hiPSC-derived neurons. (**A**) Representative image of Cal-520-loaded hiPSC-derived astrocytes at rest. (**B**) Exemplary traces depicting spontaneous activity in hiPSC-derived astrocytes. (**C**) Response to the application of BzATP (300 μM) in the abscence (black trace) and presence (red trace) of AFC-5128 (30 nM). The values represent the mean and SEM. (Paired t-test, ***p < 0.001 (n = 18). (**D**) Exemplary traces illustrating BzATP-evoked Cal-520 fluorescence responses of individual astrocytes in the abcence of AFC-5128 (30 nM). (**E**) Exemplary traces illustrating BzATP-evoked Cal-520 fluorescence responses of individual astrocytes in the presence of AFC-5128 (30 nM). (**F**) Response to the application of BzATP in the presence of 1 mM Mg^{2+} and 2 mM Ca^{2+}.

As is typical of BzATP stimulation, this elevation in $[Ca^{2+}]i$ persisted for a few seconds after the agonist was washed out. In support of the role for the P2X7R in mediating this response, 3 min pre-incubation of astrocytes with the P2X7R antagonist AFC-5128, followed by co-application of BzATP with AFC-5128 (30 nM) significantly reduced BzATP-mediated $[Ca^{2+}]i$ response (Figure 4C). Individual astrocytes responded to BzATP in a synchronous manner by increasing their Cal-520 fluoresence (ΔF), indicative of increased $[Ca^{2+}]i$ (Figure 4D). This was markedly reduced in the presence of the P2X7R antagonist, AFC-5128 (Figure E). Physiological concentration of extracellular Mg^{2+} and Ca^{2+} is known to inhibit P2X7Rs [35]. Inhibition of the P2X7R by physiological concentrations of extracellular divalent cations is a characteristic feature of this receptor [36-38]. Consistent with these findings, we found that BzATP application in the presence of 1 mM Mg^{2+} and 2 mM Ca^{2+} failed to induce any decernable increase in Cal-520 fluorescence in hiPSC-derived astrocytes (Figure 4F). These results demonstrate that Ca^{2+} entry across the plasma membrane mediated via P2X7Rs contribute to the BzATP-evoked Ca^{2+} signals and confirms the functional expression of P2X7Rs in hiPSC-derived astrocytes.

4. Discussion

Here, we differentiated hiPSC-derived cortical forebrain neurons and glia exhibiting fundamental electrophysiological properties and calcium signaling which may make them a more suitable *in vitro* model for drug screening compared to current rodent models. Using fast agonist application and simultaneous Ca^{2+} imaging, we show that while both cell types, neurons and astrocytes, respond by $[Ca^{2+}]i$ increase upon BzATP stimulation, the selective P2X7R antagonist AFC-5128 abolishes this effect confirming the functional expression of P2X7R in hiPSC-derived neurons and astrocytes.

9

341   Despite extensive investigation into neuronal and glial P2X7R expression and function in both
342 *in vitro* and *in vivo* animal models [39-41], limited studies have been conducted to characterize its
343 expression and function in human-derived neurons and astrocytes and only two studies have
344 reported the presence of *P2rx7* mRNA in cultured human adult and fetal brain tissue [29, 30]. P2X7R
345 has been proposed as a potential therapeutic target in a plethora of human conditions ranging from
346 cancer, to cardiovascular conditions to diseases of the CNS such as neurodegenerative diseases (e.g.
347 Alzheimer's disease), psychiatric diseases (e.g. schizophrenia, depression) and, more recently
348 epilepsy [42-46]. Studies investigating a causative role of P2X7R during diseases have, however, been
349 mainly restricted to experimental animal models. hiPSC-derived neurons and glia have been widely
350 accepted as human brain-relevant *in vitro* cellular models to investigate phenotypic alterations in
351 neurological diseases [25, 27, 47]. Another important consideration is the fact that P2X7R exhibits
352 remarkable species-specific differences in their pharmacological properties to drugs such as AFC-
353 5128. Thus, to advance findings from pre-clinical experimentation into the clinical setting, the
354 development of human-derived cellular models for targeted drug screening, such as that for the
355 P2X7R in this study, would serve an invaluable tool to bridge the gap between translational animal
356 models and human neurological diseases.

357   Whereas the presence of P2X7R on microglia and oligodendrocytes is well-established, whether
358 P2X7R is functional on neurons and astrocytes remains controversial [48, 49]. Data has suggested that
359 on neurons, the main site for P2X7R seems to be at presynaptic terminals [50], where it may
360 contributes to the regulation of neurotransmitter release, including GABA and glutamate [5]. Further
361 evidence of neuronal expression of the P2X7R stems from studies using *P2rx7*-EGFP (enhanced green
362 fluorescent protein) reporter mice [51] and mice expressing humanized P2X7R [52]. Other studies
363 have, however, failed to detect P2X7R on neurons [53, 54]. P2X7R has also been shown to be expressed
364 and functional on astrocytes *in vitro* and *in vivo [41]*. Moreover, P2X7R expression has been shown to
365 be increased in several disease models including in ischemia and transgenic models of Alzheimer's
366 disease [55, 56]. Similar to neurons, conflicting evidence exists on whether P2X7Rs are expressed on
367 astrocytes [54]. Our findings that both hiPSC-derived neurons and astrocytes show surface
368 expression of P2X7Rs has wide implications in signaling mechanisms in the brain. Both neurons and
369 astrocytes release ATP which is the endogenous ligand for P2X7Rs [57]. Although ATP is a low
370 affinity ligand at P2X7Rs, [57] P2X7Rs on astrocytes may be activated by ATP released from both
371 neurons and astrocytes leading to signal amplification. P2X7R activation on astrocytes could promote
372 enhanced astrocyte-mediated glutamate release leading to increased network excitability. Likewise,
373 ATP released from astrocytes could also directly activate neuronal P2X7Rs promoting hyper-
374 excitable neuronal networks. In addition, at the site of brain injury, exogenous ATP mediates the
375 release of pro-inflammatory cytokines leading to neuroinflammation via P2X7Rs [58] possibly via
376 upregulation of neuronal and/or astrocytic P2X7R during neurological conditions.

377   While our results suggest P2X7Rs to be functional on both human-derived astrocytes and
378 neurons, it is important to keep in mind that our studies are carried out under *in vitro* conditions and
379 whether P2X7Rs are expressed *in vivo* in humans requires further investigation and clarification
380 including, for example patch clamp in human brain slices. Our results do not show what neuronal
381 subtype expresses P2X7Rs, although their activation is known to affect both glutamate and GABA
382 neurotransmission, suggesting their expression on excitatory and inhibitory neurons [5].
383 Differentiation of layer-specific cortical neurons from hiPSCs has been well established [18, 59, 60],
384 allowing elucidation of the functional expression of P2X7Rs in layer-specific cortical GABAergic and
385 glutamatergic neurons derived from hiPSCs in future studies. P2X7Rs have been shown to be
386 upregulated in human reactive astrocytes [30]. We did not detect discernable changes in morphology
387 of astrocytes in culture over time, but did not assess if the culture conditions leads to
388 neuroinflammation and the generation of reactive astrocytes.

389   Finally, BzATP-evoked responses should be interpreted with caution because BzATP is a non-
390 specific agonist at purinergic receptors and agonist activity at non-P2X7Rs has also been documented.
391 Examples include BzATP-evoked responses at ionotropic P2X1, P2X2 and P2X3 [61] and
392 metabotropic P2Y2, P2Y11 and P2Y13 [62, 63]. In addition, BzATP is metabolized to other adenine

10

393 derivatives like Bz-adenosine by ecto-nucleotidases and could activate A1 receptors in tissues [64].
394 Action by BzATP metabolites is, however, highly unlikely because the drug is superfused onto the
395 recorded cells as a continuous stream of fast flowing solution and quickly removed from the imaging
396 chamber. Importantly, suggesting BzATP-mediated responses are mainly mediated mainly via
397 P2X7Rs, AFC-5128, specific P2X7R antagonist [34], suppressed calcium increases both in neurons and
398 astrocytes.
399

400   In conclusion, here we demonstrate the expression of functional P2X7Rs on hiPSCs-derived
401 neurons and astrocytes contributing further evidence for the expression of P2X7Rs in these cell types
402 and providing the proof of concept that hiPSCs represent a valid model to study P2X7Rs signaling in
403 a human cellular model.
404

415 **Conflicts of Interest:** The authors declare no conflict of interest. The funders had no role in the design of the
416 study; in the collection, analyses, or interpretation of data; in the writing of the manuscript, or in the decision to
417 publish the results. K.D. and M.H. are affiliated with Lead Discovery Center GmbH and Affectis Pharmaceuticals
418 respectively but had no influence in the study design.

419

420

421

422

423

424

425

426

427

428

429

430

431

432

433

434

435

436

437

11

References

1. Fields, R.D. and G. Burnstock, *Purinergic signalling in neuron-glia interactions.* Nat Rev Neurosci, 2006. **7**(6): p. 423-36.

2. Illes, P. and J. Alexandre Ribeiro, *Molecular physiology of P2 receptors in the central nervous system.* Eur J Pharmacol, 2004. **483**(1): p. 5-17.

3. Haydon, P.G. and G. Carmignoto, *Astrocyte control of synaptic transmission and neurovascular coupling.* Physiol Rev, 2006. **86**(3): p. 1009-31.

4. Surprenant, A., *Functional properties of native and cloned P2X receptors.* Ciba Found Symp, 1996. **198**: p. 208-19; discussion 219-22.

5. Sperlagh, B., et al., *Involvement of P2X7 receptors in the regulation of neurotransmitter release in the rat hippocampus.* J Neurochem, 2002. **81**(6): p. 1196-211.

6. Solle, M., et al., *Altered cytokine production in mice lacking P2X(7) receptors.* J Biol Chem, 2001. **276**(1): p. 125-32.

7. Goloncser, F. and B. Sperlagh, *Effect of genetic deletion and pharmacological antagonism of P2X7 receptors in a mouse animal model of migraine.* J Headache Pain, 2014. **15**: p. 24.

8. Romagnoli, R., et al., *The P2X7 receptor as a therapeutic target.* Expert Opin Ther Targets, 2008. **12**(5): p. 647-61.

9. Chen, S.P., et al., *Inhibition of the P2X7-PANX1 complex suppresses spreading depolarization and neuroinflammation.* Brain, 2017. **140**(6): p. 1643-1656.

10. Olla, I., et al., *P2X7 Receptor Upregulation in Huntington's Disease Brains.* Front Mol Neurosci, 2020. **13**: p. 567430.

11. Song, P., et al., *Increased expression of the P2X7 receptor in temporal lobe epilepsy: Animal models and clinical evidence.* Mol Med Rep, 2019. **19**(6): p. 5433-5439.

12. Wei, Y.J., et al., *Increased Expression and Cellular Localization of P2X7R in Cortical Lesions of Patients With Focal Cortical Dysplasia.* J Neuropathol Exp Neurol, 2016. **75**(1): p. 61-8.

13. Hibell, A.D., et al., *Species- and agonist-dependent differences in the deactivation-kinetics of P2X7 receptors.* Naunyn Schmiedebergs Arch Pharmacol, 2001. **363**(6): p. 639-48.

14. Donnelly-Roberts, D.L., et al., *Mammalian P2X7 receptor pharmacology: comparison of recombinant mouse, rat and human P2X7 receptors.* Br J Pharmacol, 2009. **157**(7): p. 1203-14.

15. Chessell, I.P., et al., *Cloning and functional characterisation of the mouse P2X7 receptor.* FEBS Lett, 1998. **439**(1-2): p. 26-30.

16. Humphreys, B.D., et al., *Isoquinolines as antagonists of the P2X7 nucleotide receptor: high selectivity for the human versus rat receptor homologues.* Mol Pharmacol, 1998. **54**(1): p. 22-32.

17. Norenberg, W., et al., *Positive allosteric modulation by ivermectin of human but not murine P2X7 receptors.* Br J Pharmacol, 2012. **167**(1): p. 48-66.

18. Shi, Y., et al., *Human cerebral cortex development from pluripotent stem cells to functional excitatory synapses.* Nat Neurosci, 2012. **15**(3): p. 477-86, S1.

19. Tcw, J., et al., *An Efficient Platform for Astrocyte Differentiation from Human Induced Pluripotent Stem Cells.* Stem Cell Reports, 2017. **9**(2): p. 600-614.

20. Livesey, M.R., et al., *Maturation and electrophysiological properties of human pluripotent stem cell-derived oligodendrocytes.* Stem Cells, 2016. **34**(4): p. 1040-53.

21. Douvaras, P., et al., *Directed Differentiation of Human Pluripotent Stem Cells to Microglia.* Stem Cell Reports, 2017. **8**(6): p. 1516-1524.

12

481 22. Schwartz, M.P., et al., *Human pluripotent stem cell-derived neural constructs for predicting neural toxicity.*
482   Proc Natl Acad Sci U S A, 2015. **112**(40): p. 12516-21.

483 23. Tukker, A.M., et al., *Towards animal-free neurotoxicity screening: Applicability of hiPSC-derived neuronal*
484   *models for in vitro seizure liability assessment.* ALTEX, 2020. **37**(1): p. 121-135.

485 24. Schadt, E.E., et al., *Evolving toward a human-cell based and multiscale approach to drug discovery for CNS*
486   *disorders.* Front Pharmacol, 2014. **5**: p. 252.

487 25. Rowe, R.G. and G.Q. Daley, *Induced pluripotent stem cells in disease modelling and drug discovery.* Nat Rev
488   Genet, 2019. **20**(7): p. 377-388.

489 26. Grskovic, M., et al., *Induced pluripotent stem cells--opportunities for disease modelling and drug discovery.* Nat
490   Rev Drug Discov, 2011. **10**(12): p. 915-29.

491 27. Avior, Y., I. Sagi, and N. Benvenisty, *Pluripotent stem cells in disease modelling and drug discovery.* Nat Rev
492   Mol Cell Biol, 2016. **17**(3): p. 170-82.

493 28. Lovelace, M.D., et al., *P2X7 receptors mediate innate phagocytosis by human neural precursor cells and*
494   *neuroblasts.* Stem Cells, 2015. **33**(2): p. 526-41.

495 29. Hashioka, S., et al., *Purinergic responses of calcium-dependent signaling pathways in cultured adult human*
496   *astrocytes.* BMC Neurosci, 2014. **15**: p. 18.

497 30. Narcisse, L., et al., *The cytokine IL-1beta transiently enhances P2X7 receptor expression and function in human*
498   *astrocytes.* Glia, 2005. **49**(2): p. 245-58.

499 31. Yan, Y., et al., *Efficient and rapid derivation of primitive neural stem cells and generation of brain subtype*
500   *neurons from human pluripotent stem cells.* Stem Cells Transl Med, 2013. **2**(11): p. 862-70.

501 32. North, R.A. and A. Surprenant, *Pharmacology of cloned P2X receptors.* Annu Rev Pharmacol Toxicol, 2000.
502   **40**: p. 563-80.

503 33. North, R.A., *Molecular physiology of P2X receptors.* Physiol Rev, 2002. **82**(4): p. 1013-67.

504 34. Fischer, W., et al., *Critical Evaluation of P2X7 Receptor Antagonists in Selected Seizure Models.* PLoS One,
505   2016. **11**(6): p. e0156468.

506 35. Michel, A.D., I.P. Chessell, and P.P. Humphrey, *Ionic effects on human recombinant P2X7 receptor function.*
507   Naunyn Schmiedebergs Arch Pharmacol, 1999. **359**(2): p. 102-9.

508 36. Virginio, C., et al., *Effects of divalent cations, protons and calmidazolium at the rat P2X7 receptor.*
509   Neuropharmacology, 1997. **36**(9): p. 1285-94.

510 37. Jiang, L.H., *Inhibition of P2X(7) receptors by divalent cations: old action and new insight.* Eur Biophys J, 2009.
511   **38**(3): p. 339-46.

512 38. Yan, Z., et al., *Calcium-dependent block of P2X7 receptor channel function is allosteric.* J Gen Physiol, 2011.
513   **138**(4): p. 437-52.

514 39. Alloisio, S., et al., *Functional evidence for presynaptic P2X7 receptors in adult rat cerebrocortical nerve*
515   *terminals.* FEBS Lett, 2008. **582**(28): p. 3948-53.

516 40. Rubini, P., et al., *Functional P2X7 receptors at cultured hippocampal astrocytes but not neurons.* Naunyn
517   Schmiedebergs Arch Pharmacol, 2014. **387**(10): p. 943-54.

518 41. Kaczmarek-Hajek, K., et al., *Re-evaluation of neuronal P2X7 expression using novel mouse models and a*
519   *P2X7-specific nanobody.* Elife, 2018. **7**.

520 42. Woods, L.T., et al., *Purinergic receptors as potential therapeutic targets in Alzheimer's disease.*
521   Neuropharmacology, 2016. **104**: p. 169-79.

522 43. Burnstock, G., *Purinergic Signalling: Therapeutic Developments.* Front Pharmacol, 2017. **8**: p. 661.

523 44. Di Virgilio, F., *P2X7 is a cytotoxic receptor....maybe not: implications for cancer.* Purinergic Signal, 2020.

13

524 45. Lucae, S., et al., *P2RX7, a gene coding for a purinergic ligand-gated ion channel, is associated with major*
525 *depressive disorder.* Hum Mol Genet, 2006. **15**(16): p. 2438-45.

526 46. Beamer, E., W. Fischer, and T. Engel, *The ATP-Gated P2X7 Receptor As a Target for the Treatment of Drug-*
527 *Resistant Epilepsy.* Front Neurosci, 2017. **11**: p. 21.

528 47. Karagiannis, P., et al., *Induced Pluripotent Stem Cells and Their Use in Human Models of Disease and*
529 *Development.* Physiol Rev, 2019. **99**(1): p. 79-114.

530 48. Illes, P., T.M. Khan, and P. Rubini, *Neuronal P2X7 Receptors Revisited: Do They Really Exist?* J Neurosci,
531 2017. **37**(30): p. 7049-7062.

532 49. Miras-Portugal, M.T., et al., *Neuronal P2X7 Receptor: Involvement in Neuronal Physiology and Pathology.* J
533 Neurosci, 2017. **37**(30): p. 7063-7072.

534 50. Miras-Portugal, M.T., et al., *P2X7 receptors in rat brain: presence in synaptic terminals and granule cells.*
535 Neurochem Res, 2003. **28**(10): p. 1597-605.

536 51. Jimenez-Pacheco, A., et al., *Transient P2X7 Receptor Antagonism Produces Lasting Reductions in*
537 *Spontaneous Seizures and Gliosis in Experimental Temporal Lobe Epilepsy.* J Neurosci, 2016. **36**(22): p. 5920-
538 32.

539 52. Metzger, M.W., et al., *Genetically dissecting P2rx7 expression within the central nervous system using*
540 *conditional humanized mice.* Purinergic Signal, 2017. **13**(2): p. 153-170.

541 53. Sim, J.A., et al., *Reanalysis of P2X7 receptor expression in rodent brain.* J Neurosci, 2004. **24**(28): p. 6307-14.

542 54. Jabs, R., et al., *Lack of P2X receptor mediated currents in astrocytes and GluR type glial cells of the hippocampal*
543 *CA1 region.* Glia, 2007. **55**(16): p. 1648-55.

544 55. Martin, E., et al., *New role of P2X7 receptor in an Alzheimer's disease mouse model.* Mol Psychiatry, 2019.
545 **24**(1): p. 108-125.

546 56. Franke, H., et al., *Pathophysiology of astroglial purinergic signalling.* Purinergic Signal, 2012. **8**(3): p. 629-
547 57.

548 57. Surprenant, A., et al., *The cytolytic P2Z receptor for extracellular ATP identified as a P2X receptor (P2X7).*
549 Science, 1996. **272**(5262): p. 735-8.

550 58. Ferrari, D., et al., *The P2X7 receptor: a key player in IL-1 processing and release.* J Immunol, 2006. **176**(7): p.
551 3877-83.

552 59. Qi, Y., et al., *Combined small-molecule inhibition accelerates the derivation of functional cortical neurons from*
553 *human pluripotent stem cells.* Nat Biotechnol, 2017. **35**(2): p. 154-163.

554 60. Espuny-Camacho, I., et al., *Pyramidal neurons derived from human pluripotent stem cells integrate efficiently*
555 *into mouse brain circuits in vivo.* Neuron, 2013. **77**(3): p. 440-56.

556 61. Bianchi, B.R., et al., *Pharmacological characterization of recombinant human and rat P2X receptor subtypes.*
557 Eur J Pharmacol, 1999. **376**(1-2): p. 127-38.

558 62. Fedorov, I.V., O.A. Rogachevskaja, and S.S. Kolesnikov, *Modeling P2Y receptor-Ca2+ response coupling in*
559 *taste cells.* Biochim Biophys Acta, 2007. **1768**(7): p. 1727-40.

560 63. Carrasquero, L.M., et al., *P2X7 and P2Y13 purinergic receptors mediate intracellular calcium responses to*
561 *BzATP in rat cerebellar astrocytes.* J Neurochem, 2009. **110**(3): p. 879-89.

562 64. Kukley, M., et al., *Ecto-nucleotidases and nucleoside transporters mediate activation of adenosine receptors on*
563 *hippocampal mossy fibers by P2X7 receptor agonist 2'-3'-O-(4-benzoylbenzoyl)-ATP.* J Neurosci, 2004. **24**(32):
564 p. 7128-39.

565